

# ANISOTROPIC PROPERTIES OF FIBER/MATRIX INTERFACE TRANSITION ZONE

SHAN HE\* AND EN-HUA YANG†

\* Nanyang Technological University  
Singapore  
e-mail: heshan@ntu.edu.sg

† Nanyang Technological University  
Singapore  
e-mail: ehyang@ntu.edu.sg

**Key words:** Fiber reinforced concrete, Interfacial transition zone (ITZ), Sample preparation, Nanoindentation, Anisotropy

**Abstract:** A new approach to characterize interface transition zone (ITZ) between microfiber and cement matrix is reported. The approach allows the ITZ to be exposed through the longitudinal direction of fiber axis, which enable mechanical tests of the ITZ from 2 mutually perpendicular directions. Results show that the ITZ between microfiber and cement matrix is highly heterogeneous along its axial direction and can extend up to 100  $\mu\text{m}$  from the interface into the matrix, suggesting the perturbation due to inclusion of microfibers to packing of cement grains is severer than that due to inclusion of aggregates. Mechanical properties of ITZ between microfiber and cement matrix are anisotropic. Stiffness and ductility of ITZ in the radial direction are 31% and 28% higher than that in the tangential direction, respectively.

## 1 INTRODUCTION

The interfacial transition zone (ITZ) between an inclusion (*e.g.*, aggregate) and bulk matrix in cement-based composites has been the focus of extensive research [1, 2]. It has been well accepted and documented that the ITZ is quite different in its microstructure, composition and mechanical properties than the bulk cement matrix. Formation of the ITZ is usually attributed to the ‘wall’ effect [3], which describes the inability of cement grains to pack around the inclusion as densely as they do in the bulk matrix, resulting in higher water-to-cement ratio around the inclusion. Thus, the ITZ is more porous and weaker compared to the bulk matrix, and in many cases governs the mechanical properties and durability of cement-based materials.

The influence of ITZ may be amplified when microfibers are included in the cement matrix

because microfibers have high aspect ratio, and thus much larger surface area. The ITZ between microfiber and cement-based matrix largely determines the pullout behavior of the fiber from the surrounding matrix [4], which in turn controls the composite performance [5]. Characterization of fiber/matrix interfacial properties thus is the key to understand the fracture process that occurs at the fiber/matrix interface and in the ITZ.

While the ITZ between aggregate and cement paste have been well studied [1, 2], there are only few studies reporting the ITZ between microfiber and cement-based matrix. Even among the limited number of studies, the results are sometimes contradictory [4, 6] and the properties that determined in these studies are not the most relevant properties controlling the behavior of the ITZ during fiber pullout. This is because that established methods for studying the ITZ often perform analyses on 2-D cross-

sectional plane that intersect with fiber axis. The results obtained by this method have two issues. First, the results can hardly be representative, because the variability of the ITZ along its longitudinal direction cannot be avoided [7]. Disagreement among published literatures on the subject matter may be due to this reason. Second, the properties of the ITZ can only be analyzed in its axial direction. It is known that circumferential compressive normal stresses due to matrix shrinkage give rise to the frictional pullout resistance of fiber (Figure 1a). Thus, mechanical properties of ITZ in radial direction (*i.e.*,  $xx$  direction) are mostly relevant to the circumferential compressive normal stresses (Figure 1b and 1c). New approach to extract relevant and representative information of the ITZ is therefore needed.

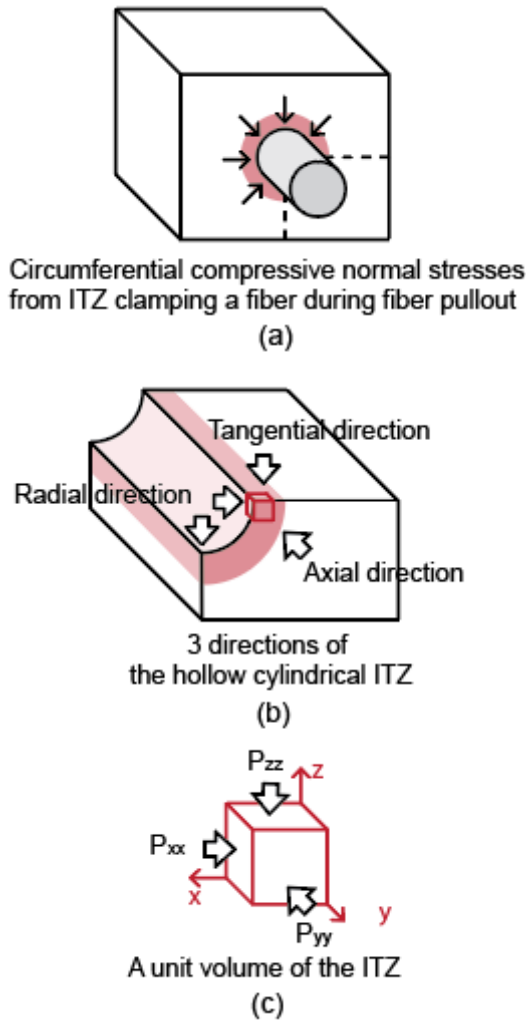


**Figure 1:** Schematic illustration of the 3 directions of the ITZ surrounding a microfiber.

To address the research gaps mentioned above, this paper reports a new approach to quantitatively characterize the ITZ between microfiber and cement matrix. Instead of probing the properties in a small annular ITZ from the axial ( $yy$ ) direction on the cross-sectional plane perpendicular to the fiber axis, we exposed the ITZ along the longitudinal direction of the fiber axis as shown in Figure 2a and the properties of ITZ were characterized from the tangential ( $zz$ ) direction on the large ITZ plane parallel to the fiber axis and from the radial ( $xx$ ) direction on the interior surface of the fiber groove. In the following sections, methods for sample preparation is presented first, followed by ITZ characterization by means of backscattered electron (BSE) imaging and nano-indentation.

## 2. MATERIAL AND METHODS

### 2.1 Material

In this study, CEM I 52.5 N Portland cement was used to prepare a cement paste with a  $w/c$  of 0.2 as the matrix. The microfiber used to produce the ITZ is a polyethylene (PE) microfiber (Spectra® 1000, Honeywell) with a diameter of  $23\ \mu\text{m}$ . Table 1 summarizes the physical properties and geometry of PE fibers used in this study.

**Table 1:** Properties of the PE fibers

Diameter ( $\mu\text{m}$ )	Length (mm)	Tensile strength (MPa)	Elastic modulus (GPa)	Density ( $\text{g}/\text{cm}^3$ )
23	19	3250	113	0.96

### 2.2 Sample preparation

To obtain sufficiently large ITZ area for examination, longitudinal section passing through the central axis of the fiber is prepared for ITZ characterization (Figure 2a). As can be seen, long rectangular cross-sections of ITZ and the empty fiber groove (*i.e.*, the interior surface of the hollow cylindrical ITZ) are exposed. This configuration allows the study of the ITZ from two mutually perpendicular directions, *i.e.*, tangential ( $zz$ ) direction and radial ( $xx$ ) direction, by performing tests on the rectangular

cross-sections of ITZ and on the fiber groove, respectively.

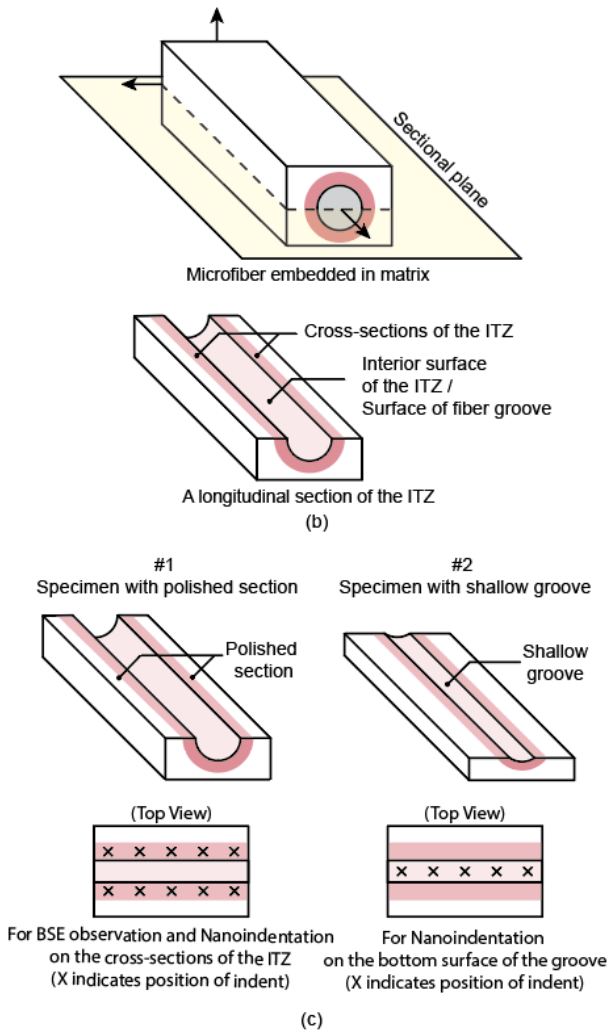


**Figure 2:** Schematic illustration of (a) a longitudinal section of the ITZ containing rectangular cross-sections of the ITZ and an empty fiber groove and (b) 2 types of specimens for nanoindentation tests.

Two types of specimens were prepared for ITZ characterization as schematically illustrated in Figure 2b. Specimens with polished section (Figure 2b, left) are prepared for BSE imaging to determine the gradient of anhydrous cement in the ITZ and for nano-indentation to evaluate mechanical properties of the ITZ in the tangential (zz) direction. Specimens with shallow groove (Figure 2b, right) are prepared for nano-indentation on the fiber groove to reveal mechanical properties of the ITZ in the radial (xx) direction.

To prepare the specimen, a long PE fiber was cut into about 150 mm in length and fixed at the

center of a prismatic mold. The fresh cement paste was prepared and cast into the mold (Figure 3a, top), which were then covered with plastic sheets and cured in air at room temperature for one day. The hardened specimens were removed from the molds and cured in lime-saturated water for another 27 days in the laboratory at a temperature of  $23 \pm 3^\circ\text{C}$  before further processing.

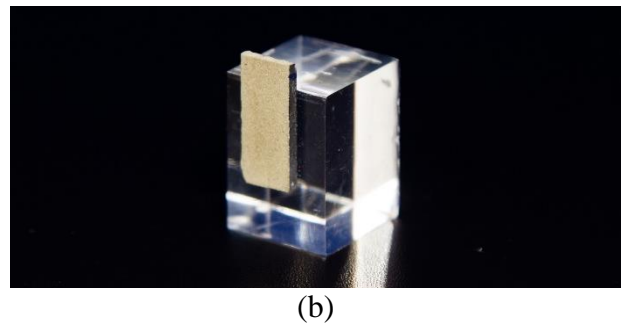
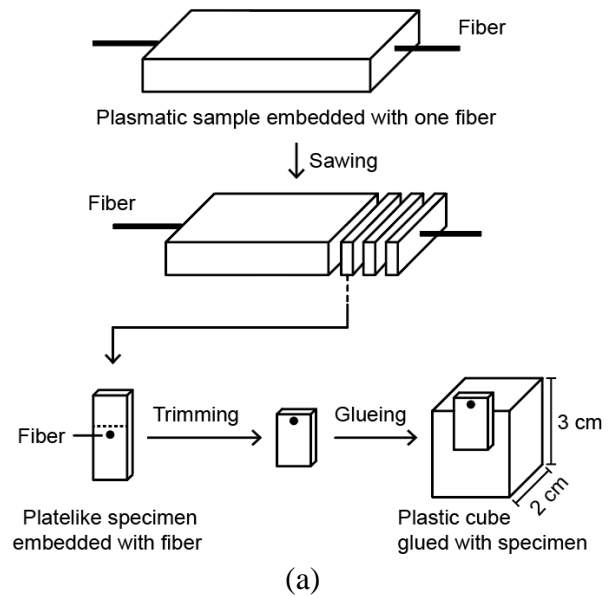


**Figure 3:** (a) Preparation of a mounted specimen, and (b) overview photograph of the mounted specimen.

The cement paste prism embedded with one continuous fiber was then sliced into thin plate-like specimens of 1 mm thick (Figure 4a, middle). Each resulting specimen would have a segment of fiber embedded in its center position perpendicular to its front surface (Figure 4a, bottom). The thin plate-like specimen was then trimmed down from the top to the dashed line in Figure 3 (bottom), which is roughly 1 mm above the fiber. The trimmed specimen was then glued to a plastic cubic holder (Figure 3b), allowing the removal of material from the uppermost. In

this study, for specimens with polished section, the grinding was stopped at exactly the center of the fiber. **Figure 4a** shows an SEM micrograph of a specimen during grinding, in which the embedded fiber was half exposed. For the specimens with shallow groove, the grinding was controlled with great care to craft a shallow groove to allow the indenter reaching the bottom of the groove (**Figure 4b**).

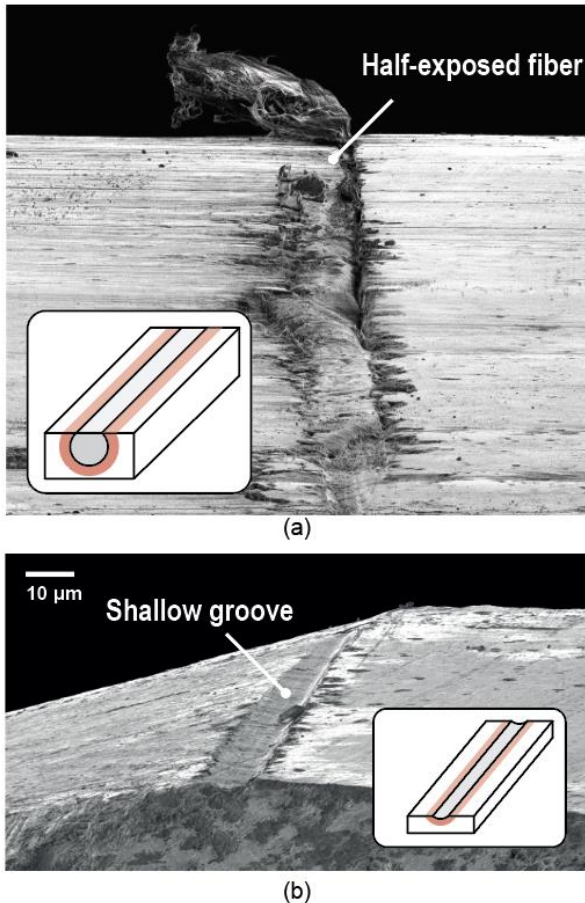


**Figure 4:** SEM micrograph of a specimen (a) during grinding and (b) after the groove depth reduction.

An in-house designed grinding and polishing system, which consists of a rotary machine on the top facing downwards and a precise z-axis stage (accuracy: 10 μm) on the bottom as shown in **Figure 5**, was developed for the controlled grinding. The rotary machine and the z-axis stage are fixed firmly onto a frame to minimize the vibration during operation. The rotary machine is used to drive a lapping wheel attached with abrasive media and operates at speeds up to 35,000 revolutions per minutes. The specimen (on holder) was glued to an

alumina plate fixed on the z-axis stage by screws (**Figure 5**). By increasing the height of the z-axis stage and forcing the top surface of the specimen to contact the rotating wheel, the abrasive could therefore travel across the sample surface and grind the surface by pushing, rolling, and scratching behaviors of the abrasives. In this study, P1200 grit abrasive paper is used for flattening the fracture surface, and P2500 grit abrasive paper is used for slowly reaching desired section. After grinding, the specimen is cleaned in isopropyl alcohol in an ultrasonic bath for 1 min.

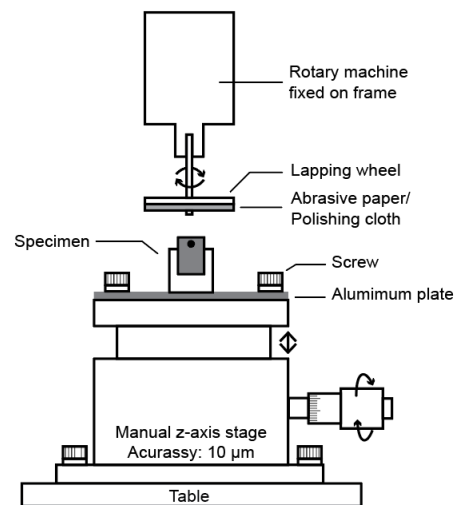


**Figure 5:** Schematic illustration of the set-up used for grinding and polishing.

To further improve the quality of the surface finishing, the specimen is polished by using the same set-up in the same manner but with a polishing wheel. The wheel was mounted with a synthetic silk polishing cloth (VerduTex from Buehler) charged with 1 μm diamond paste. The advantage of using only one size of diamond has been described in [8]. Ethanol and 1,4 butanediol (1:1) was also charged onto the cloth to dissipate any heat built-up. Similarly, increase of the height of the z-axis stage should be slow during polishing as well. 3 to 5 seconds of polishing time is sufficient to yield a smooth surface. Extended duration has negative effects because the debris removed from the specimen surface could easily accumulated on the polishing cloth, resulting in deep scratches on the specimen. After polishing, the specimen is then cleaned in an ultrasonic bath again for 1

min.

Figures 6a and 6b show the typical optical microscope images of a specimen after grinding and polishing, respectively, in which a fiber groove at the center of the specimen was exposed. As can be seen, the groove is preserved and the ITZ along the groove is visually as smooth as the bulk matrix away from the groove. Figure 6c shows a SEM micrograph of the same specimen after polishing, in which a region near the end of the groove was scanned by AFM. Figure 6d shows the AFM image of this 40  $\mu\text{m}$  by 40  $\mu\text{m}$  region, it can be seen that the scanned area except for the groove is uniformly flat. The calculated average root-mean-squared (RMS) roughness of the flat region in this figure and several regions randomly selected around the groove is 59.47 nm, which satisfies the criteria for nano-indentation as proposed in published literature [8]. The sample preparation method developed in this study reveals large ITZ region with high quality finishing which enables the study of the ITZ from tangential (zz) direction and radial direction by performing test on the rectangular cross-sections of ITZ and fiber groove, respectively (Figure 3).

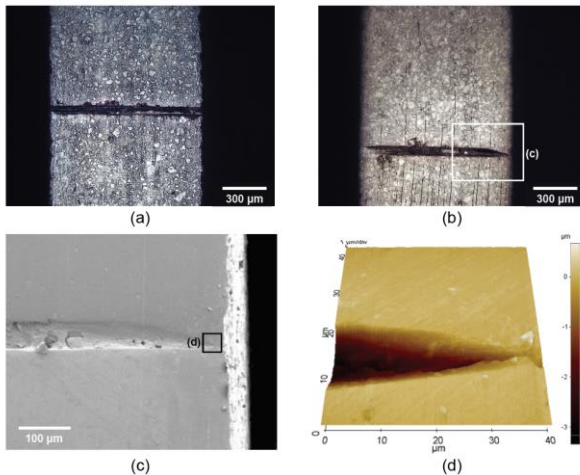


**Figure 6:** Optical microscope images of a specimen (a) after grinding and (b) after polishing, (c) SEM micrograph and (d) AFM scanning of a polished section with fiber groove.

## 2.3 Characterization techniques

### 2.3.1 BSE image analysis

BSE image analysis has been well established as a quantitative method for the

study of concrete microstructure [1, 9-11]. In BSE images, contrast in grey level is produced primarily by mean atomic number variations of different phases, which enables both the discrimination of individual microstructural components and the assessment of their spatial distribution. Figure 7a shows an SEM micrograph of an ITZ specimen with polished section. Figure 7b shows the BSE image of the same specimen, which was made by electronically ‘stitching’ eight BSE images taken at a nominal magnification of  $\times 500$  to ensure high resolution of the image. Contrast in the BSE image yields clear definition of constituents, *e.g.*, the region in light gray corresponds to the anhydrous cement. Figure 7c shows the binary image with black pixels representing the anhydrous cement after post-image processing. The area fraction of anhydrous cement in each band ( $10 \times 1000 \mu\text{m}^2$ ) was determined by calculating the percentage of black pixels over all pixels in the band. A total of 5 specimens with identical groove length of 1 mm were examined.

### 2.3.2 Nano-indentation

Mechanical properties of the ITZ were investigated by means of an Agilent G200 Nano Indenter fitted with a Berkovich tip. Indentation tests were carried out by depth-sensing techniques with the continuous stiffness measurements (CSM) option, which allows the hardness and elastic modulus to be recorded as a function of contact depth in a single indentation. A detailed description of the CSM depth-sensing tests and analysis method can be found in [12].

Nano-indentations were carried out on the large rectangular cross-sections of ITZ in specimens with polished section to evaluate mechanical properties of the ITZ in the tangential (zz) direction (Figure 2c, left). The indentation depth for each test was set to be 500 nm. The mean hardness and the mean modulus of each indent were determined from the CSM indentation curve by averaging the hardness (or modulus) value between 100 nm and 500 nm indentation depth. For each specimen, several lines of indents were produced parallel to the

edge of the fiber groove with a spacing of  $10\ \mu\text{m}$  as shown in the inset of **Figure 7a**. After the nano-indentation tests, all specimens were investigated by both SE image and BSE image analyses. From BSE images, the corresponding phase where each indent was produced was subsequently revealed. The indents on anhydrous cement grains were deliberately excluded for only the properties of the hydration product in the ITZ is of interest to this study. From SE images, the distance of the indents to the fiber groove could be determined. The indents were categorized into 4 groups according to their respective distance, *i.e.*,  $0\text{--}10\ \mu\text{m}$ ,  $10\text{--}20\ \mu\text{m}$ ,  $20\text{--}30\ \mu\text{m}$ , and  $30\text{--}40\ \mu\text{m}$ , from the fiber/matrix interface. For each group, at least 50 indents were included and statistically evaluated.

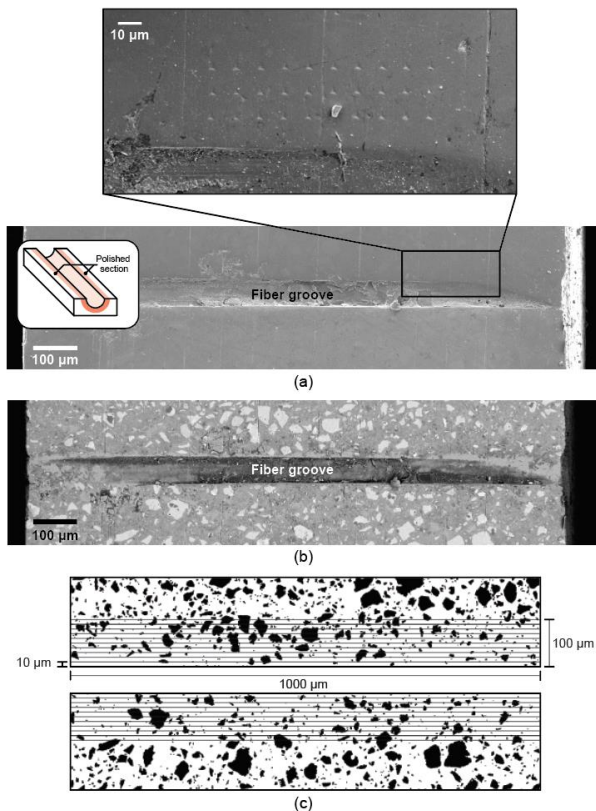


**Figure 7:** (a) SEM micrograph of specimen with polished surface containing a fiber groove, with the inset showing residual indents on a cross-section of the ITZ, (b) BSE image of the same specimen, and (c) binary image converted from the BSE image with the grids indicating the bands.

Nano-indentations were carried out on the empty fiber groove in specimens with shallow

groove to evaluate mechanical properties of the ITZ in the radial (xx) direction (**Figure 2c, right**). The tests were carried out to a maximum indentation depth of  $1000\ \text{nm}$ . The mean hardness and the mean modulus of each test were determined from the CSM indentation curve by averaging the hardness (or modulus) value between  $200\ \text{nm}$  and  $1000\ \text{nm}$  indentation depth. The spacing is set to be  $20\ \mu\text{m}$ . At least 60 indents were included and statistically evaluated.

## RESULTS AND DISCUSSION

### 3.1 Anhydrous cement in the ITZ

**Figure 8** shows the variation in volume fraction of anhydrous cement adjacent to microfibers based on the BSE imaging analysis. As can be seen, volume fraction of anhydrous cement increases with increasing distance from fiber/matrix interface. The increment rate is high within  $0\text{--}40\ \mu\text{m}$  from the interface, rising to about 20%. Moderate increment is observed beyond  $40\ \mu\text{m}$ , reaching to around 26% at  $100\ \mu\text{m}$  from the interface, which could be considered as the bulk matrix. It has been reported that the volume fraction of anhydrous cement for a cement paste with same w/c of 0.2 is around 30% [13], which is in good agreement of the current results.

The results suggest that the microstructure of the hydrated cement paste is highly modified in the vicinity of microfibers, extending up to  $100\ \mu\text{m}$  from the interface into the matrix with the most significant deficit in anhydrous cement being in the region of about  $40\ \mu\text{m}$  adjacent to the fiber. The zone with a reduced amount of anhydrous cement surrounding a fiber is even wider than that around aggregates, which has been published as in a range of  $50\ \mu\text{m}$  [2]. This may be due to that aggregates have curved and uneven surfaces, which facilitate the packing of cement grains to some extent. The long microfiber, however, is perfectly flat and thus may have acted more effectively as a ‘wall’, resulting in a poor packing in the vicinity of interface and a wider apparent width of the ITZ. In fact, it has been reported that the geometric interactions between particles and fibers are

also strongly affected by the aspect ratio and the rigidity of the fiber [14, 15], indicating the perturbation created by the fibers maybe more complicated than that created by aggregates.

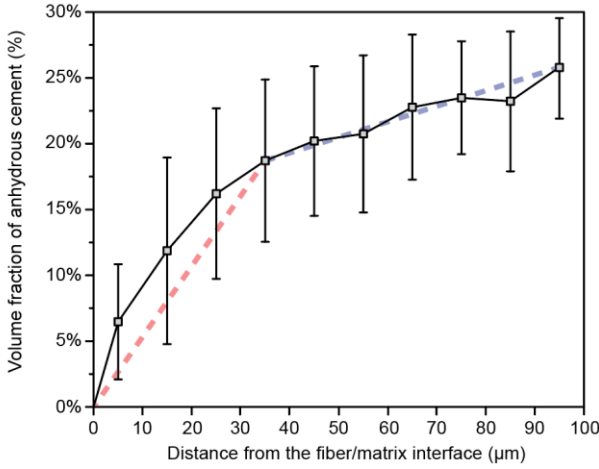


**Figure 8:** Volume fraction of anhydrous cement at different distances from the fiber/matrix interface.

### 3.2 Nano-mechanical response of the ITZ

Figure 9 presents typical CSM nano-indentation curves measured from the tangential (zz) and the radial (xx) directions. As can be seen, indentation modulus measured from the tangential (zz) direction remains steady after an initial fluctuation which could be attributed to the surface texture of the fiber groove. However, indentation modulus measured from the radial (xx) direction increases with increasing indentation depth. This suggests the ITZ between microfibers and cement matrix in the current study may have a concentric laminated microstructure, which may be due to the ‘one-sided’ growth of hydrates [16].

Figures 10 plots the mean modulus and the mean hardness measured from the tangential (zz) direction as a function of distance from fiber/matrix interface and the mean modulus and the mean hardness measured from the radial (xx) direction. As can be seen, both the mean elastic modulus and the mean hardness increase with increasing distance from fiber/matrix interface. The mean elastic modulus in the 0-10 μm region is only 77% that of the 20-40 μm region from the interface. It should be noted that the mechanical properties presented here are only the properties of hydration products in the

ITZ, for the results of indents on anhydrous cement grains were deliberately excluded. The real properties of the ITZ, which consists of hydration products and anhydrous cement, should be influenced by both the properties of the hydration products and the relative proportion of anhydrous cement. Thus, since the volume fraction of the anhydrous cement also increase with increasing distance from fiber/matrix interface (Figure 8), the overall gradients of the mechanical properties of the ITZ are expected to be steeper.

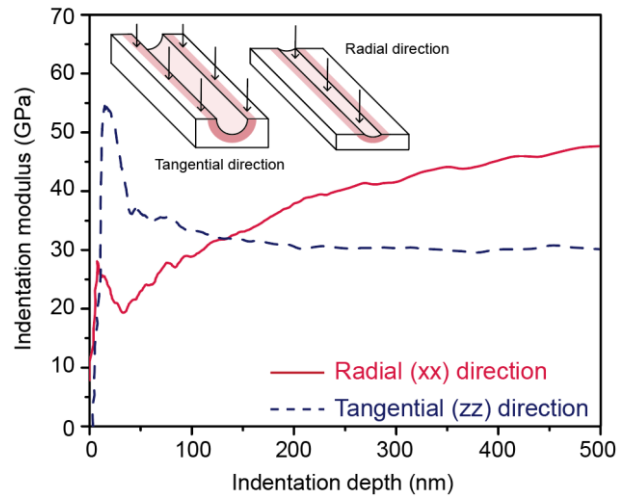


**Figure 9:** Typical CSM nano-indentation curves measured from the tangential (zz) direction and the radial (xx) direction.

In addition, the variation of both the modulus and the hardness in the 0-10 μm region are the largest compared to other regions, demonstrating again the microstructure developed near the fiber is highly heterogeneous. The implication of this could be significant because during fiber debonding or pullout, microcracks would preferably initiate from the weakest regions in the ITZ. Thus, it is plausible that this weak and highly heterogeneous 10-μm-wide region near the interface is the most critical zone that governs the load transfer and composite performance. This may also suggest that strengthening of the ITZ should target for this region.

The mean modulus and the mean hardness measured from the radial (xx) direction are  $37.09 \pm 10.20$  GPa and  $1.48 \pm 0.53$  GPa, respectively, as shown in Figures 10a and 10b

(the leftmost boxes). As the properties in the radial (xx) direction are more relevant to the circumferential compressive normal stresses that give rise to the frictional pullout resistance of fiber, they should be used to describe the ability of the ITZ to resist decay or failure during the process of fiber pullout. Furthermore, the average radial (xx) modulus ( $37.09 \pm 10.20$  GPa) is 31% higher than the average tangential (zz) modulus near the interface (0-10  $\mu\text{m}$ :  $28.23 \pm 13.03$  GPa). This suggests mechanical properties in the ITZ are anisotropic.

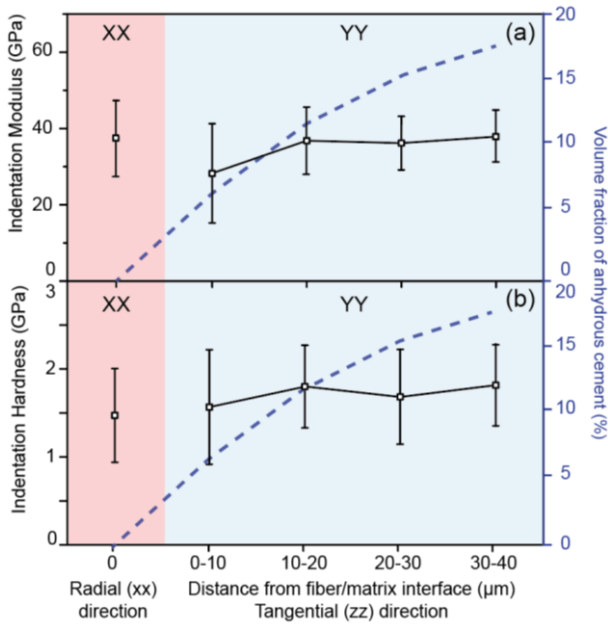


**Figure 10:** (a) Mean modulus and (b) mean hardness of the ITZ measured from the radial (xx) and the tangential (zz) directions.

It should be noted that the degree of anisotropy measured in current study is an average property of the volume of material sensed by indenter during indentation. As the ITZ has a concentric graded microstructure, its properties are expected to change continuously in its radial direction, and thus the degree of anisotropy within the unit volume may not necessarily be a constant value, but most likely to be a function of the distance from the interface. However, estimation of the plasticity or elasticity gradient of compositionally graded materials through indentation is much more complicated and requires priori-knowledge of the graded material such as its average Poisson ratio and experimentally-determined load-

displacement curves of indentation performed at homogeneous materials which comprise the phases of the graded layers [17-20], which are all currently unavailable. More comprehensive studies on the property gradient of the ITZ are needed to obtain a more quantitative understating to determine the best resolution for the quantification of the anisotropy of the ITZ.

### 3.3 Anisotropic properties of the ITZ

To further investigate this anisotropic response, the mean modulus is plotted against the mean hardness of each indent measured from the tangential (zz) direction as well as from the radial (xx) direction (Figure 11). As can be seen, with a given mean hardness, the mean radial (xx) modulus is higher than the mean tangential (zz) modulus, *i.e.*, the ITZ is stiffer in the radial direction than the tangential direction. The mean modulus-to-hardness (M/H) ratio (*i.e.*, slope of the fitted curve in Figure 11) can be used to assess ductility of material [21, 22] because it represents the spatial extent of the elastic deformation that might occur under loading before permanent yielding occurs in the indentation test [23]. As can be seen, the mean radial (xx) M/H ratio (24) is 28% higher than the mean tangential (zz) M/H ratio (18.8), suggesting that the yield strain of the ITZ is anisotropic as well and the ITZ from the radial direction is more ductile than that from the tangential direction.

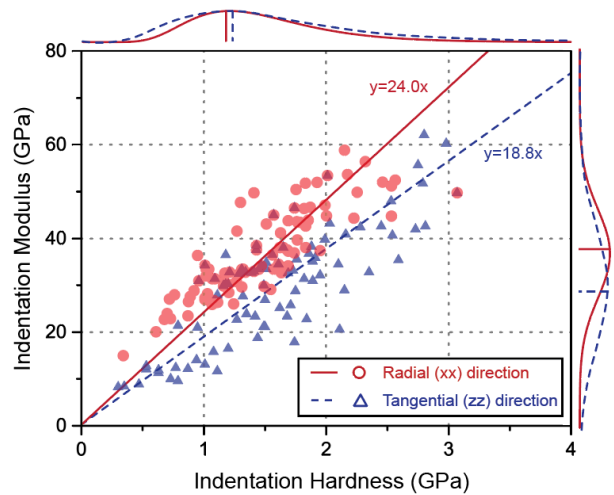


**Figure 11:** Mean modulus and mean hardness of each indent measured from the tangential (zz) direction and the radial (xx) direction.

The anisotropic response of the ITZ seems to be a reasonable consequence of having a concentric laminated microstructure as indicated by the CSM curve (Figure 9). Furthermore, the precipitation of calcium hydroxide in the ITZ may have also contributed to this anisotropic effect. Figure 12 shows a fractured section of the ITZ. As can be seen, large crystals with a size of around 20  $\mu\text{m}$  formed preferably against the fiber/matrix interface. In the study of the ITZ between aggregate and cement based matrix, it has been reported that there is a preferential orientation of calcium hydroxide with the c-axis parallel to the aggregate surface [24], which is consistent to the results of current study. Further study is necessary to reveal the exact origins of the anisotropic properties of the ITZ.

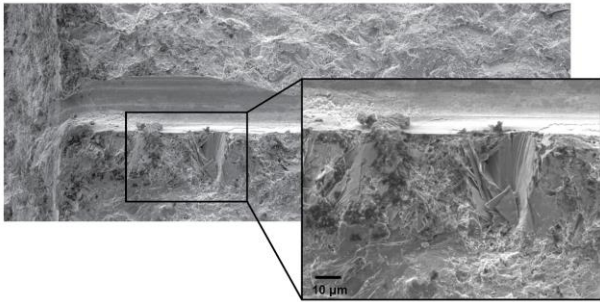


**Figure 12:** SEM micrograph of a fractured section of the ITZ with inset showing the calcium hydroxide crystals formed in the ITZ.

The anisotropic behavior of the ITZ between microfiber and cement matrix is significant. Firstly, understanding this behavior may facilitate the study of the failure mechanisms of the interfacial bond between fiber and cement matrix. Secondly, it is also expected to enhance the predictability of existing analytical and numerical models for fiber-reinforced concrete, in which the ITZ is treated as isotropic. Lastly, it should be noted this anisotropic response should not be exclusive to the ITZ surrounding microfibers. The ITZ between aggregate and cement paste may also be anisotropic. Future studies are needed to address the effects of anisotropy on the overall performance of concrete.

## CONCLUSIONS

A new approach was proposed to quantitatively characterize the ITZ between microfiber and cement matrix and to reveal its anisotropic properties. In this study, the ITZ between PE microfiber and cement paste was characterized from the tangential (zz) direction on the large ITZ plane parallel to the fiber axis and from the radial (xx) direction on the interior surface of the fiber groove. A sample preparation method revealing the ITZ along the longitudinal direction of the fiber with high quality surface finishing was developed. The gradient of anhydrous cement, and mechanical properties of the ITZ were studied by means of SE imaging, BSE imaging and nano-indentation.

Results show that the ITZ can extend up to 100  $\mu\text{m}$  from the interface into the matrix with the most significant deficit in anhydrous cement in the region of about 40  $\mu\text{m}$  adjacent to the fiber. The larger extent of the ITZ suggests that perturbation due to the inclusion of microfibers to the packing of cement grains is severer than that due to the inclusion of aggregates. Furthermore, the ITZ between microfiber and cement matrix is highly heterogeneous along its axial direction. Thus, existing ITZ analysis methods performed on the 2-D cross-sectional plane intersecting with fiber axis can lead to errors and uncertainties. Mechanical properties of ITZ between microfiber and cement matrix are anisotropic. Stiffness and ductility of the ITZ in the radial (xx) direction are 31% and 28% higher than that in the tangential (zz) direction, respectively. Further study is necessary to reveal the exact origins of the anisotropic properties of the ITZ and to address potential effects of ITZ anisotropy on the overall performance of cement-based composites.

## REFERENCES

- [1] K.L. Scrivener, A.K. Crumbie, P. Laugesen, The interfacial transition zone (ITZ) between cement paste and aggregate in concrete, *Interface science*, **12** (2004) 411-421.
- [2] J. Ollivier, J. Maso, B. Bourdette, Interfacial transition zone in concrete, *Advanced Cement Based Materials*, **2** (1995) 30-38.
- [3] D. Pinchin, D. Tabor, Interfacial phenomena

- in steel fibre reinforced cement I: Structure and strength of interfacial region, *Cement and concrete research*, **8** (1978) 15-24.
- [4] Y.-W. Chan, V.C. Li, Effects of transition zone densification on fiber/cement paste bond strength improvement, *Advanced cement based materials*, **5** (1997) 8-17.
- [5] V.C. Li, H. Stang, Interface property characterization and strengthening mechanisms in fiber reinforced cement based composites, *Advanced cement based materials*, **6** (1997) 1-20.
- [6] A. Katz, A. Bentur, Mechanical properties and pore structure of carbon fiber reinforced cementitious composites, *Cement and concrete research*, **24** (1994) 214-220.
- [7] H. Elias, D.M. Hyde, An elementary introduction to stereology (quantitative microscopy), *Am J Anat*, **159** (1980) 412-446.
- [8] M. Miller, C. Bobko, M. Vandamme, F.-J. Ulm, Surface roughness criteria for cement paste nanoindentation, *Cement and Concrete Research*, **38** (2008) 467-476.
- [9] K.L. Scrivener, H. Patel, P. Pratt, L. Parrott, Analysis of phases in cement paste using backscattered electron images, methanol adsorption and thermogravimetric analysis, *MRS Online Proceedings Library Archive*, **85** (1986).
- [10] K.L. Scrivener, Backscattered electron imaging of cementitious microstructures: understanding and quantification, *Cement and Concrete Composites*, **26** (2004) 935-945.
- [11] K. Scrivener, R. Snellings, B. Lothenbach, *A practical guide to microstructural analysis of cementitious materials*, Crc Press 2016.
- [12] X. Li, B. Bhushan, A review of nanoindentation continuous stiffness measurement technique and its applications, *Materials characterization*, **48** (2002) 11-36.
- [13] M. Vandamme, F.-J. Ulm, P. Fonollosa, Nanogranular packing of C-S-H at substochiometric conditions, *Cement and Concrete Research*, **40** (2010) 14-26.
- [14] F. De Larrard, *Concrete mixture proportioning: a scientific approach*, CRC Press 2014.
- [15] N. Roussel, *Understanding the rheology of concrete*, Elsevier 2011.
- [16] E.J. Garboczi, D.P. Bentz, Digital simulation of the aggregate-cement paste interfacial zone in concrete, *Journal of materials Research*, **6** (1991) 196-201.
- [17] I. Choi, M. Dao, S. Suresh, Mechanics of indentation of plastically graded materials—I: Analysis, *Journal of the Mechanics and Physics of Solids*, **56** (2008) 157-171.
- [18] I. Choi, A. Detor, R. Schwaiger, M. Dao, C. Schuh, S. Suresh, Mechanics of indentation of plastically graded materials—II: Experiments on nanocrystalline alloys with grain size gradients, *Journal of the Mechanics and Physics of Solids*, **56** (2008) 172-183.
- [19] A. Giannakopoulos, S. Suresh, Indentation of solids with gradients in elastic properties: Part II. Axisymmetric indentors, *International Journal of Solids and Structures*, **34** (1997) 2393-2428.
- [20] A. Giannakopoulos, S. Suresh, Indentation of solids with gradients in elastic properties: Part I. Point force, *International Journal of Solids and Structures*, **34** (1997) 2357-2392.
- [21] C.G. Hoover, F.-J. Ulm, Experimental chemo-mechanics of early-age fracture properties of cement paste, *Cement and Concrete Research*, **75** (2015) 42-52.
- [22] M.A. Qomi, K. Krakowiak, M. Bauchy, K. Stewart, R. Shahsavari, D. Jagannathan, D.B. Brommer, A. Baronnet, M.J. Buehler, S. Yip, Combinatorial molecular optimization of cement hydrates, *Nature communications*, **5** (2014) 4960.
- [23] A.C. Fischer-Cripps, *Nanoindentation*, Springer New York 2013.
- [24] J. Larbi, J. Bijen, Orientation of calcium hydroxide at the Portland cement paste-aggregate interface in mortars in the presence of silica fume: A contribution, *Cement and Concrete Research*, **20** (1990) 461-470.